Hindawi
Complexity
Volume 2020, Article ID 8810663, 12 pages
https://doi.org/10.1155/2020/8810663

Research Article

Locomotion Prediction for Lower Limb Prostheses in Complex Environments via sEMG and Inertial Sensors

Fang Peng,[1,2] **Cheng Zhang**,[3] **Bugong Xu**,[2] **Jiehao Li**,[4] **Zhen Wang**,[4] **and Hang Su**[4]

[1]*University of Electronic Science and Technology of China, Zhongshan Institute, Zhongshan 528402, China*
[2]*School of Automation Science and Engineering, South China University of Technology, Guangzhou 510641, China*
[3]*Department of Computer Science and Communications Engineering, Waseda University, Tokyo, Japan*
[4]*Department of Electronics, Information and Bioengineering, Politecnico di Milano, Milano 20133, Italy*

Correspondence should be addressed to Hang Su; hang.su@polimi.it

Received 30 August 2020; Revised 15 October 2020; Accepted 22 November 2020; Published 4 December 2020

Academic Editor: Rongxin Cui

Previous studies have shown that the motion intention recognition for lower limb prosthesis mainly focused on the identification of performed gait. However, the bionic prosthesis needs to know the next movement at the beginning of a new gait, especially in complex operation environments. In this paper, an upcoming locomotion prediction scheme via multilevel classifier fusion was proposed for the complex operation. At first, two motion states, including steady state and transient state, were defined. Steady-state recognition was backtracking of a completed gait, which would be used as prior knowledge of motion prediction. In steady-state recognition, surface electromyographic (sEMG) and inertial sensors were fused to improve recognition accuracy; five typical locomotion modes were recognized by random forest classifier with over 97.8% accuracy. The transient state was defined as an observation period at the initial stage of upcoming movement, in which only the sEMG signal was recorded due to the limitation of sliding window length. LightGBM classifier was validated to outperform other methods in the accuracy and prediction time of transient-state recognition. Finally, a simplified HMM model based on prior knowledge and observation result was constructed to predict upcoming locomotion. The results indicated that the locomotion prediction was over 91% accuracy. The proposed scheme implements the locomotion prediction at the initial stage of each gait and provides critical information for the gait control of lower limb prosthesis.

1. Introduction

The powered lower limb prosthesis, which can provide active torque for amputees and imitate the movement of healthy human leg better than a passive prosthesis, has been widely studied for a decade [1–4]. For developing powered lower limb prostheses, one major challenge is how to recognize the current locomotion mode of amputee and further identify the motion intention of amputee under complex scenarios [5–7] so as to realize the seamless transition of different locomotive tasks and then control lower limb prostheses with correct parameters. Otherwise, the actual trajectory or torque of the lower limb prostheses will deviate from expectations. For example, the actual terrain is upstairs, but the prostheses controller still uses the control parameters in level walking, which will lead to discomfort for amputees and even the risk of falling down. Therefore, it is necessary to consider the suitable control method for safe locomotion.

Therefore, several sensors, especially electromyogram and mechanical sensors, have been widely used for locomotion detection. Surface electromyography (sEMG) signals can adequately represent the action state of the corresponding muscle group; many researchers used them as the only control input to recognize human locomotion [8–12]. Huang et al. [8] used the sEMG signals of two gluteal muscles and nine residual thigh muscles to realize the gait phase classification. However, sEMG signals are susceptible to skin sweat, muscle fatigue, and physical illness of subjects.

Thus, other researchers have tried to confirm that a set of different mechanical sensors could identify locomotion modes [13–15]. These mechanical sensors can be commonly classified into two groups: kinematic sensors and kinetic sensors. The former included angular, velocity, acceleration, etc. The latter included interaction force or torque between user and prosthesis (or environment). In [16], the sensor system consisted of an accelerometer and a gyroscope, respectively, located on the prosthetic pylon and two pressure sensors under the prosthetic foot. In [17], three six-axis IMUs were employed for identifying different locomotion. Although mechanical sensors are more easily embedded in lower limb prostheses than sEMG, they are challenging to achieve onset prediction alone [18]. Compared to the physical data from the prostheses or sound side leg, the sEMG signal can directly reflect the volitional control of the human body. A few studies have fused both mechanical information and sEMG signals to recognize locomotion modes. On the basis of the sEMG signals mentioned above [8], the authors added a 6-DOF load cell mounted on the prosthetic socket for better identifying continuous locomotion modes. Ai et al. [19] fused sEMG and accelerometer signals to classify five lower limb's motions. Additionally, Young et al. [20] compared the contribution of sEMG sensors and mechanical sensors embedded on powered prostheses and found that the recognition accuracy obtained by sEMG and inertial sensors (a six-axis inertial measurement unit (IMU) located on the shank) was significantly higher than that of other sensors. These results have indicated that multisensor fusion can obviously improve classification accuracy; especially, sEMG sensor and inertial sensor fusion is encouraging [21, 22]. Thus, the remaining problem is how to utilize the sensors to predict upcoming locomotion modes, which is essential for the powered prosthesis to actuate the artificial joints correctly.

In most previous work, the recognition of locomotion intention was accomplished by collecting and analyzing multisensor signals before the critical events of gait, such as heel contact or toe off, which denote the beginning of the stance phase or swing phase. At the same time, a lot of pattern recognition schemes have been studied in gait recognition. In [23], a transition period about 300–650 ms was reported before critical events for locomotion switch, and support vector machine (SVM) was used as a classifier. In another study [20], four 300 ms windows were extracted before critical events of the stance and swing phase, and a dynamic Bayesian network (DBN) classification algorithm was employed to recognize movement intention. In [24], the authors proposed a forward predictor to identify and respond to the user's intent, built an adaptive sEMG model, and added the label of backward estimation into forwarding predictor, and they extracted a 300 ms window of data before a gait event for forward prediction and used DBN and linear discriminant analysis (LDA) as forward and backward classifiers, respectively. However, these intention recognition methods mainly focused on the recognition of the performed gait or the transitional movement had been occurred. In fact, when the lower limb prosthesis led by the amputee's residual limb moves, whether the next phase is the stance phase of weight acceptance of the swing phase of lifting leg, the lower limb prosthesis should know the upcoming movement before action. If an amputee is walking slowly or intermittently, it is not accurate to predict the next step based entirely on the prior gait.

In this paper, an intention prediction scheme in complex environment via sEMG and inertial sensors fusion is proposed to recognize five locomotion modes at gait initiations. We expanded the previous studies from the following aspects:

(1) A multilevel classifier fusion strategy that combines prior gait information and current observation was proposed to infer the amputee's intent for switch control of lower limb prostheses.

(2) The designed prediction scheme provided decision at the initiations of each stance phase and swing phase.

(3) Surface EMG from four thigh muscles and inertial sensors located on thigh and shank were fused to recognize locomotion modes. The contribution of each sensor in gait recognition was studied.

(4) The pattern recognition schemes, including two traditional algorithms and two ensemble learning algorithms, were analyzed. Besides, several feature extraction and reduction dimension methods are discussed.

2. Experiments and Data Processing

2.1. Experimental Protocol. The previous gait recognition experiment has been conducted on the able-bodied subjects [17, 25] or amputee subjects wearing prothesis [26–28]. In this study, we recruited five able-bodied subjects between 20 to 50 years old, and one 31-year-old male subject with unilateral amputations was also recruited. The study was conducted following the ethical approval of confidential research involving human participants, and the protocol was approved by the University of Electronic Science and Technology of China, Zhongshan Institute (Project identification code is 2016A020220003).

Surface EMG signals were recorded from the key thigh muscles: rectus femoris, lateral thigh muscle, medial thigh muscle, and biceps femoris, which were verified to be effective for gait recognition in [1]. The locations for electrode placements are shown in Figure 1; the center spacing for electrodes is about 3 cm. The sEMG signals were collected from all subjects with a 16-channel EMG sensor (Myomove) and uploaded to the processing system with a sampling frequency of 1024 Hz. The processing system filtered sEMG signals with a comb filter and an IIR bandpass filter. The former was selected to offset the noise of the 50 Hz band. The latter signals are between 10 and 500 Hz. The inertial sensors including two nine-axis IMUs (Witmotion JY-901) were located on the thigh and shank, respectively. Each JY-901 integrated a triaxial gyroscope, a triaxial accelerometer, and a triaxial geomagnetic survey. With the addition of the geomagnetic sensor, JY-901 can obtain more accurate triaxial posture information than the six-axis IMU by

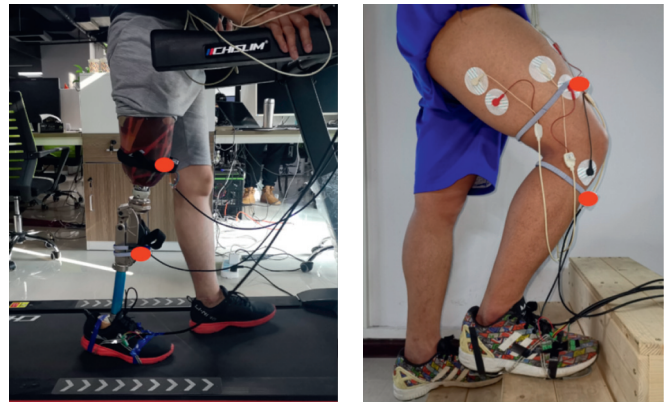

(a) (b)

Figure 1: Experiments of different locomotion: (a) level walking; (b) stair ascend.

eliminating the accumulation error of direction angle. IMU signals were collected at 200 Hz and filtered with a dynamic Kalman filter.

A pressure sensor detected critical events of gait. Two pressure sensors (FlexiForce-A201) were placed, respectively, on the heel and the first metatarsal of the subject's forefoot. The pressure sensor information is uploaded to the processing system through an acquisition card, and the sampling frequency is 700 Hz.

After receiving instructions and training, each subject was asked to complete five locomotion modes at a natural, average speed. Level walking was tested on the treadmill. Ramp ascent and ramp descent were collected with the aid of a treadmill. We used the treadmill to build a ramp with a slope of about 20 degrees. All subjects were asked to walk on these three terrains three times, one minute at a time. Stair ascends and stair descends were tested on a 3-step staircase, as shown in Figure 1. Each subject was asked to go up and down the stairs 30 times. All subjects should rest for 5 minutes between different locomotion modes to avoid the influence of muscle fatigue on the experiment and ensure the objectivity and accuracy of the experimental data.

2.2. sEMG Signal Acquisition via Compressed Sensing. Compressed sensing is a signal acquisition framework that could reduce the data storage much lower than that with conventional Nyquist sampling rate. The reduction in data storage or sampling rate could reduce the energy dissipation for the battery-powered wearable sEMG sensor. Moreover, the data deluge problem and the urgency in communication bandwidth could be lightened as well [9].

The work in [29] reported that the sEMG signal is sparser in the transform domain than that in the time domain, and the Daubechies wavelet basis can be chosen as the more appropriate selection for the sparse basis compared with DCT and Haar wavelet basis [30]. Under the framework of compressed sensing, the following linear equation holds:

$$y = \Phi\Psi s + n = Hs + n, \tag{1}$$

where $y \in \mathbb{R}^{M\times 1}$ and $s \in \mathbb{R}^{N\times 1}$ denote the undersampled sEMG measurement and the sparse representation of the sEMG signal in the Daubechies wavelet basis. Note $M < N$ is met under compressed sensing. $\Phi \in \mathbb{R}^{M\times N}$ and $\Psi \in \mathbb{R}^{N\times N}$ stand for the Bernoulli random sampling matrix and the Daubechies wavelet sparse basis, respectively, and $H = \Phi\Psi \in \mathbb{R}^{M\times N}$. $n \in \mathbb{R}^{M\times 1}$ represents the error term occurring from measurement noise and modeling error from sparse representation.

The sparse representation s is solved using the heterogeneous Bayesian compressed sensing (HBCS) algorithm, which has shown superior performances than orthogonal matching pursuit (OMP), basis pursuit (BP), and Bayesian compressed sensing (BCS) in our previous work [31–34]. In HBCS, all the unknowns are taken as random variables and follow certain probability distributions. Here each element of s is considered to be iid (identically independent distribution) and assumed to meet the following zero-mean Gaussian distribution, and the reciprocal of the variance in Gaussian distribution is then imposed by gamma distribution; the two-layer hierarchical prior distribution is shown as follows:

$$\begin{cases} P(s|\alpha) = \prod_{i=1}^{N} N\left(s_i|0, \alpha_i^{-1}\right), \\ P(\alpha|a,b) = \prod_{i=1}^{N} \text{Gamma}\left(\alpha_i|a,b\right), \end{cases} \tag{2}$$

where α_i^{-1} is the variance of the Gaussian distribution and a and b are the user-defined shape and scale parameters in the Gamma distribution. The noise n is also restricted by a two-layer hierarchical iid distribution, which is presented as

$$\begin{cases} P(n|\beta) = \prod_{i=1}^{M} N\left(n_i|0, \beta_i^{-1}\right), \\ P(\beta|c,d) = \prod_{i=1}^{M} \text{Gamma}\left(\beta_i|c,d\right), \end{cases} \tag{3}$$

where β_i^{-1} is the reciprocal of the noise variance and c and d are also used to characterize the shape and scale parameters in gamma distribution.

The conditional distribution is also allocated with Gaussian distribution as follows:

$$P(y|st;n\beta) = N\left(y|Htsn, qB^{-1}\right), \tag{4}$$

where $B = \mathrm{diag}(\beta)$, $\beta = [\beta_1, \beta_2, \ldots, \beta_M]^T$. The posterior estimation is obtained by seeking for the maximum-a-posterior (MAP) solution, which is expressed as

$$\begin{aligned} P(s|y,\alpha,\beta) &= \frac{P(y|s;\beta)P(s|\alpha)}{P(y,\alpha,\beta)}, \\ &= \frac{P(y|s;\beta)P(s|\alpha)}{\int P(y|s;\beta)P(s|\alpha)\mathrm{d}s}, \\ &= (2\pi)^{-(M/2)}|\Sigma|^{-(1/2)}\exp\left[-\left(\frac{1}{2}\right)(s-\hat{s})^T\Sigma^{-1}(s-\hat{s})\right], \end{aligned} \tag{5}$$

where $\hat{s}$ and Σ are represented as follows:

$$\begin{aligned} \hat{s} &= \Sigma H^T B y, \\ \Sigma &= \left[H^T B H + A\right]^{-1}, \end{aligned} \tag{6}$$

where $A = \mathrm{diag}(\alpha)$, $\alpha = [\alpha_1, \alpha_2, \ldots, \alpha_N]^T$ and $B = \mathrm{diag}(\beta)$, $\beta = [\beta_1, \beta_2, \ldots, \beta_M]^T$. For the hyperparameters α and β, they are learned from the measured sEMG signal by performing a type-II maximum likelihood (ML) or evidence procedure. The update formulas are expressed as follows:

$$\begin{cases} \alpha_i = \dfrac{\gamma_i + 2(a-1)}{\hat{s}_i^2 + 2b}, \\ \beta_i = \dfrac{1 + 2(c-1)}{\left(y_i - H_i\hat{s}\right)^2 + tr\left(\Sigma H_i^T H_i\right) + 2d}, \end{cases} \tag{7}$$

where $\gamma_i = 1 - \alpha_i\Sigma_{ii}$ with Σ_{ii} representing the ith diagonal element of Σ, $\hat{s}_i$ is the ith element of $\hat{s}$, and H_i is the ith row of H. Detailed derivation of the above Bayesian inference procedure has been omitted here (the readers can refer to [31, 35, 36] and the references therein).

After the sparse representation $\hat{s}$ is reconstructed, the estimated sEMG signal x is then obtained via the following transform.

$$x = \Psi\hat{s}. \tag{8}$$

2.3. Data Acquisition. In this paper, we defined two states for collecting sensor data: steady state and transient state. The steady state referred to a completely performed gait. The transient state was a short transitional period when subjects began new gait. The division of the states depended on the identification of the gait phase by pressure signal, as shown in Figure 2(a). The stance phase began when the foot touched the ground (i.e., heel contact) and terminated at the foot off the ground (i.e., toe off). The swing phase was from toe off to heel contact. Two different frames of the sliding window were designed to process the steady-state and the transient-state information separately. For steady-state recognition, i.e., state backtracking, which was used to identify performed gaits, a sliding window covering a full stride cycle was designed. The steady state was from the heel contact to next heel contact or from the toe off to next toe off, as shown in Figure 2(b), in which, sEMG and IMU sensors were fused to analyze performed locomotion mode. For transient state, the shorter the time of the data acquisition window, the better the smooth control of lower limb prosthesis. Therefore, a 50 ms small sliding window with only sEMG signal recorded was designed at every initial of the heel contact and toe off. Three reasons for choosing 50 ms sEMG signal were (1) the sEMG signal generally precedes mechanical signal at responding to movement onset; (2) it takes about 20 ~ 50 ms for human muscles to respond to an action potential; and (3) due to the limitation of IMU signal acquisition frequency, only several data could be recorded within 50 ms, which might lead to confusion for identification. During the transient state, the control system of the powered prosthesis also used the previous gait controller, which means that the response of the prothesis was at least 50 ms slower than that of the healthy leg. This delay time is relatively short compared with the whole cycle, which will not have an adverse effect on the walking status of the powered prothesis but can ensure the accuracy of the next state control.

2.4. Feature Extraction

2.4.1. Feature Extraction of sEMG Signals. To take into account the timeliness of signal processing, the time-domain feature extraction method for sEMG was considered in this work [37]. In preliminary work [12], over 20 features of sEMG signals were quantitatively compared, and the following enumerated features were optimal time-domain feature groups for gait recognition.

(i) Slope sign change (SSC).

SSC characterizes the frequency information of sEMG signals:

$$\mathrm{SSC} = \sum_{i=2}^{N-1} f\left((x_i - x_{i+1}) * (x_i - x_{i-1})\right), \tag{9}$$

where $f(x) = \begin{cases} 1, & \text{if } x > Th_{\mathrm{SSC}} \\ 0, & \text{if } x \le Th_{\mathrm{SSC}} \end{cases}$. We set the threshold Th_{SSC} to 40 mV.

(ii) Willison amplitude (WAMP).

WAMP refers to the number of times that the difference of sEMG signal amplitude between adjacent two points exceeds a predetermined threshold and is related to the level of muscle contraction.

$$\mathrm{WAMP} = \sum_{i=1}^{N} \mathrm{sgn}\left(\left|x_{i+1} - x_i\right| - Th_{\mathrm{WAMP}}\right). \tag{10}$$

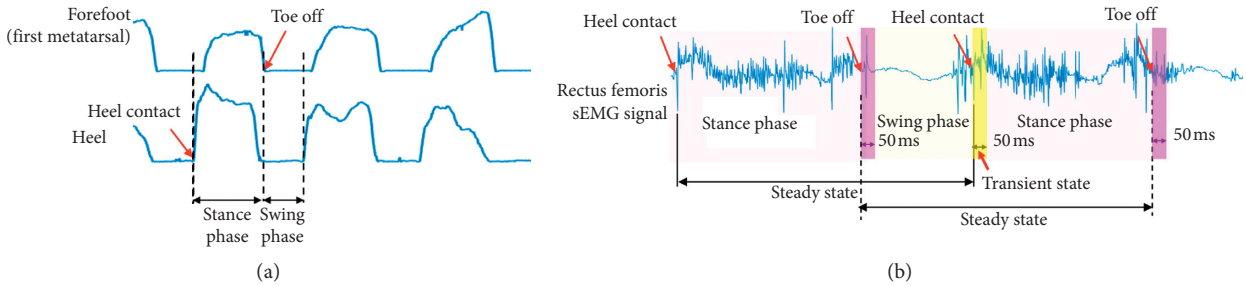

Figure 2: Data processing methods. (a) Gait phase detection by pressure sensors. (b) Sliding window scheme and definition.

The parameter Th_{WAMP} is optimized by experimental comparison, and we obtain the optimized Th_{WAMP} value of 50 mV.

(iii) Waveform length (WL).

Waveform length is the cumulative length of the waveform at a given time.

$$\mathrm{WL} = \sum_{i=1}^{N-1} \left| x_{i+1} - x_i \right|. \tag{11}$$

(iv) Logarithmic variance (LogVAR).

Variance is the average of the deviation square of the variable. However, the average of the sEMG signal is close to zero. Therefore, the variance of sEMG is generally replaced by the following formula:

$$\mathrm{VAR} = \frac{1}{N-1} \sum_{i=1}^{N} x_i^2. \tag{12}$$

In order to make the variance have better normal distribution characteristics, the logarithm of the variance was extracted as a new feature, which was defined as LogVAR.

2.4.2. Feature Extraction of IMU Signals. A multifeature fusion method is proposed to extract the feature vectors of IMU signals. This method can express the motion characteristics of lower limbs more comprehensively and effectively and provide a guarantee for the better training classification model.

(i) Discrete wavelet transform (DWT).

DWT was used to decompose the filtered IMUs data. After wavelet decomposition, the high- and low-frequency coefficients were extracted in time domain to obtain more comprehensive and clearer pattern information and to eliminate the influence of noise further. Wavelet decomposition decomposed the IMU signal into high-frequency details and low-frequency approximation. For gait information, the low-frequency component is quite important and contains the main characteristics of the signal, while the high-frequency component gives the details or differences of the signal. The approximate value $A_j[n]$ (i.e., low frequency part) and detail part $D_j[n]$ (i.e., high frequency part) of the decomposed original signal are formulated as

$$A_{j+1}[n] = \sum_k A_j[n] h(2n-k), D_{j+1}[n] = \sum_k A_j[n] g(2n-k), \tag{13}$$

where $h(\cdot)$ means scale function coefficient, $g(\cdot)$ presents wavelet function coefficient, and j represents the scale of decomposition.

By experimental comparison, Daubechies 9 was selected to decompose acceleration and angular velocity signals and extract the characteristic values of wavelet transform coefficients. Furthermore, the time-domain features of the high- and low-frequency coefficients were extracted, including absolute mean (MAV) and standard deviation (STD).

(ii) Cross-correlation coefficient.

The cross-correlation function can extract and analyze the correlation characteristics of different periodic signals or quasiperiodic signals [38, 39]. Therefore, in the human locomotion pattern recognition, the characteristic parameters of different locomotion modes can be represented by the correlation characteristics of different inertial signals.

The cross-correlation function describes the correlation between two random signals $X(t), Y(t)$ at any time. It is given by

$$R_{XY} = \frac{(1/n-1)\sum_{i=1}^{n}(X_i - \overline{X})(Y_i - \overline{Y})}{\sqrt{\sum_{i=1}^{n}(X_i - \overline{X})^2}\sqrt{\sum_{i=1}^{n}(Y_i - \overline{Y})^2}}, \tag{14}$$

where $\overline{X}$ and $\overline{Y}$ denote the average value of a sequence frame and n is the number of samples. We calculated the correlation coefficients of the acceleration and angular velocity between the thigh and shank as the features.

2.5. Feature Reduction Dimension. The feature extraction from the sEGM and IMU signals produced the data of 68 dimensions. To improve the characterization ability of features, we obtain more valuable information and reduce the computational cost of the classification algorithm, and a lower dimensionality should be acquired by dimension

reduction. In this paper, two common dimension reduction approaches were considered: principal component analysis (PCA) and linear discriminant analysis (LDA). PCA is the most classical and widely used dimension reduction algorithm in information fusion. The basic idea of PCA is to retain the main features in the original data (the covariance structure of the data) and map the data from the high-dimensional feature space to the low-dimensional feature space by linear projection. LDA is a supervised linear dimensionality reduction method, which considers the labels of classes and facilitates the discrimination of the data after dimensionality reduction. Both methods were proved to be effective in biometric pattern recognition [40–42].

3. Intention Recognition and Locomotion Prediction Method

Locomotion prediction for the powered lower prosthesis refers to make accurate decisions of upcoming human motion based on sensor information. In this paper, a multilevel classifier fusion scheme was proposed to predict the motion intention as shown in Figure 3. The locomotion prediction system combined the steady-state recognition with transient-state recognition. The former is the backtracking of completed gait, and the latter is a preliminary identification of the upcoming gait. Then, a HMM model as a decision fusion model was designed to fuse the recognition of the steady state and transient state, the result of which is the prediction of locomotion mode.

3.1. Steady-State Recognition. In order to improve the recognition accuracy, the recognizer of the steady state was accomplished based on the fusion of sEMG and inertial signals. A variety of classifiers have been approached for intent pattern recognition. In this paper, we evaluated the performance of four classification algorithms, which include support vector machine (SVM), quadratic discriminant analysis (QDA), light gradient boosting machine (LightGBM), and random forest (RF). The SVM is a machine learning algorithm based on the statistical learning theory. The classification performance of SVM has been proved to be better than that of LDA in sEMG pattern recognition for prosthetic legs [23]. QDA is a variant of LDA, allowing nonlinear separation of data with small computation and high efficiency. The QDA classification had higher classification accuracies than LDA in classifying intention of the knee motion. [43]. LightGBM and RF are both ensemble learning algorithms that train different classifiers (weak classifiers) and then assemble these weak classifiers to form a more reliable final classifier (robust classifier). Compared to the single model learning method, ensemble learning algorithms are more likely to obtain high accuracy and generalization. LightGBM is a distributed framework of the gradient boosting decision (GBDT) tree algorithm. It was proposed by the Microsoft team's Guolin Ke et al. in 2017 to solve the problem of GBDT computing efficiency. Compared with other traditional classifiers, the LightGBM classifier performed well in the accuracy and prediction time of gait phase recognition based on sEMG [44]. Random forest is also a conventional classification algorithm with a decision tree as the base learner. Random forest has a strong anti-interference ability and is more suitable for processing high-dimensional data than SVM. Random forest has been validated to recognize five types of locomotion of lower limbs and obtain better accuracy than SVM.

3.2. Transient-State Recognition. Transient state is defined as the observation period for a motion switch, during which the lower limb prosthesis detects the upcoming movement. Because of the real-time requirement, a challenge was put forward for recognition accuracy and time. If the recognition time is too long, the prosthetic locomotion mode will be inconsistent with the actual walking terrain, which will lead to the amputee walking unnaturally. In the four classification algorithms mentioned above, QDA and LGBM have the advantage of fast computation speed in a single classification model and ensemble learning model, respectively. All four classifiers were compared and analyzed for transient-state recognition.

3.3. Locomotion Prediction. Locomotion switch is a response on account of the actual walking terrain, while pedestrian facilities of roads or buildings have an extreme regularity. The transition of various terrain is not random. Generally, the ends of a flight of stairs are usually flat, not ramps. Similarly, the ends of a ramp are usually flat, too, not stairs. Therefore, there is a certain probability of human gait switch, as shown in Table 1. For example, the current gait is level walking (LW), and then the next gait is level walking (LW), ramp ascend (RA), ramp descend (RD), stair ascend (SA), or stair descend (SD) with a probability of 20% each. If the prior gait is SA, then the next gait is LW or SA, with the probability of 50% each.

In this way, the recognition of gait intention is transformed into a probabilistic model construction problem. The next gait state recognition process can be described as a typically hidden Markov model (HMM) with strong prior knowledge. HMM is a probability model about time sequence. For human walking, a transition from one gait to another gait is a hidden process that cannot be directly observed, but the observations in transient state can be used to infer the gait transition. In this paper, the first-order HMM was utilized to fuse the backtracking gait information and the transient-state information to achieve the final locomotion prediction.

4. Results and Discussion

4.1. Steady-State Recognition Performance. Four classifiers with PCA and LDA dimensional reduction were conducted based on sEGM and IMU fusion. Recognition evaluation was performed using 10-fold cross validation. A Bayesian method based on tree-structured Parzen estimator (TPE) was utilized to solve the hyperparameter optimization problem for RF and LightGBM classifiers. SVM and QDA parameters were optimized by the grid search method.

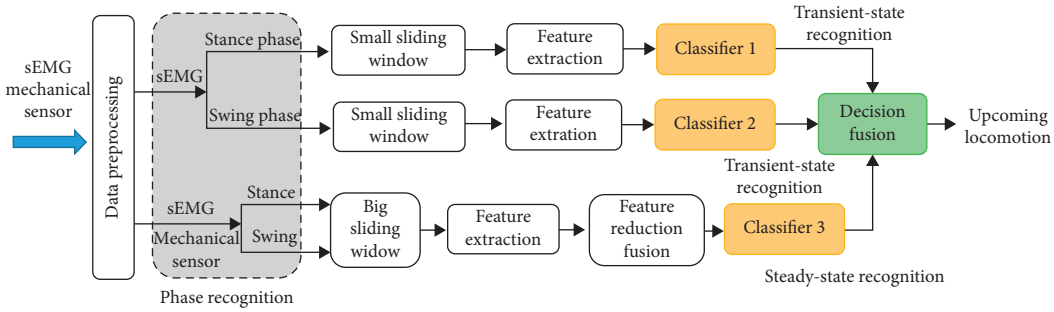

Figure 3: Architecture of the locomotion prediction scheme.

Table 1: Transition probability between locomotion modes.

	LW	RA	RD	SA	SD
LW	20	20	20	20	20
RA	50	50	0	0	0
RD	50	0	50	0	0
SA	50	0	0	50	0
SD	50	0	0	0	50

Note. LW, level walking; RA, ramp ascend; RD, ramp descend; SA, stair ascend; SD, stair descend.

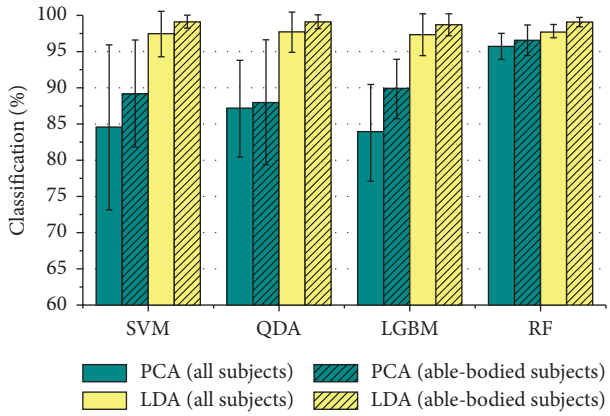

Figure 4: Steady-state accuracy with different dimension reduction methods and classifiers in different subject groups. Error bars represent ± SD.

Different subject groups, including all subjects and subjects except amputee (i.e., only able-bodied subjects), were compared. The experimental results are shown in Figure 4. In view of the dimensionality reduction algorithm, although different methods had different effects on the classifiers, LDA was more favorable for the accuracy of the classifier than PCA. RF algorithm represented good fusion performance for both dimensional-reduction methods. After LDA dimensional reduction, the classification accuracy of four classifiers was all over 99% for 5 able-bodied subjects. When the data from the amputee subject were added, the accuracy dropped slightly by 2%, but it was also over 97.4%. That means there was a discrepancy in walking posture between a healthy person and a lower limb amputee. In general, LDA + RF was the optimal combination with the highest classification accuracy, 99.1% for five able-bodied subjects and 97.8% for all six subjects. It is worth noting that all the following results are for all subjects.

The contribution of different sensors or sensor combinations in gait recognition of multisource information perception was analyzed. The IMU and sEMG signals were compared and analyzed, respectively. The result in terms of misclassification for all subjects was reported, as shown in Figure 5. For the steady-state recognition, the effect of using the IMU sensor alone was better than that of using the sEMG signal alone. The recognition accuracy of using IMUs on the thigh or shank alone was the range from 81.3% to 85%; after the combination of the two IMUs, the recognition rate was greatly improved to above 95%. It could be concluded that for improving the identification of lower limb movement identification, it was very significant to detect both the thigh and shank mechanical signals at the same time due to the difference in the movement of them. Furthermore, after the sEMG signal was combined with two IMU signals, the recognition rate continued to be improved by 1 ~ 2%. That means that the multisensor fusion is beneficial and useful for gait recognition.

Actually, different sensor signals had different effects on recognition algorithms. When only using the sEMG signal, the error rate of LDA + LGBM and LDA + RF was lower than the others. However, whatever sensor signals were used, the LDA + RF method had the lowest classification error. From the aforementioned results, there was an essential correlation between the selection of human gait recognition methods and the sensors used in the detection.

The confusion matrix from four classifiers was derived from analyzing the specific situation of the misclassification. It can be seen from Figure 6 that the accuracy of four classifiers in distinguishing five locomotion modes was in the range of 95 ~ 100%. The misclassification of all classifiers mainly occurred between the level walking and ramp ascend.

4.2. Transient-State Recognition Performance. The 50 ms sEMG signals of 4 channels were collected from the heel contact (i.e., beginning of stance phase) and toe off (i.e., beginning of swing phase) moment, respectively. The features of SSC, WAMP, WL, and LogVAR were extracted for classification recognition. After repeated verification, the feature dimensionality reduction could not significantly improve the classification accuracy. Consequently, classifiers were directly trained by utilizing the features data, which

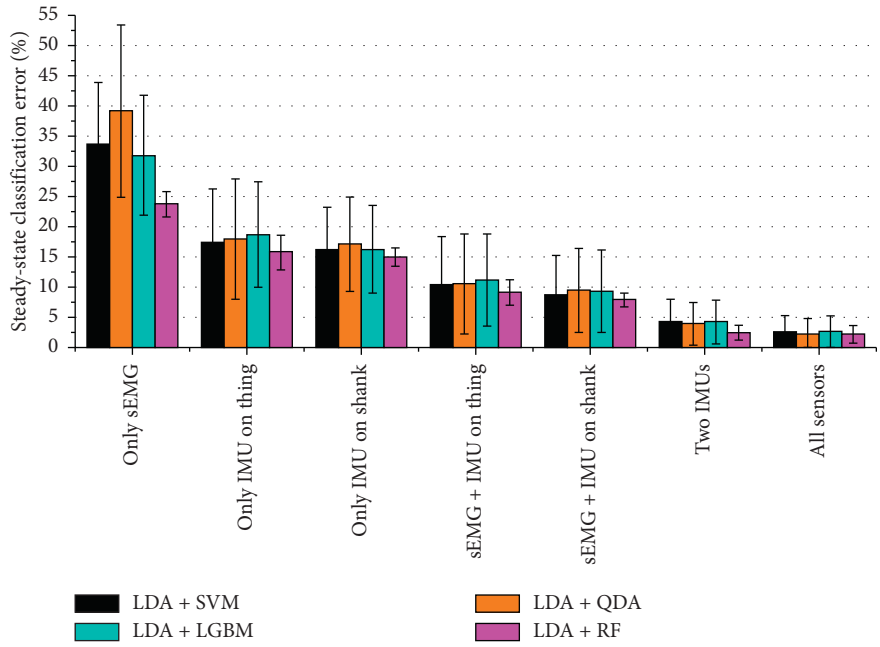

Figure 5: Contributions of different sensors and sensor combinations. Error bars represent ± SD.

would obviously shorten the data processing time. Using 10-fold cross validation, the average prediction accuracy and prediction time are shown in Table 2. Whether in the preswing or the prestance, the recognition accuracy of the LightGBM algorithm was higher than that of other classifiers. Even though the QDA algorithm had the shortest prediction time, the accuracy was the lowest. On account of gradient-based one-side sampling (GOSS) and exclusive feature bundling (EFB) techniques, LightGBM has a faster speed without lowering its accuracy. The average classification accuracy of different types of locomotion in transient state is shown in Figures 7 and 8. On the whole, the ramp ascend movement can be most accurately detected. When moving up or down the stairs, the sEMG signal at the prestance phase could be distinguished more easily, probably because the muscle stretching and contraction are more obvious in this stage.

Furthermore, we take the confusion matrix of LightGBM recognition in preswing as an example to analyze the distribution of misidentification. The confusion matrix is described in Table 3. It can be seen that stair descent movement had the highest classification error in the preswing phase, 23% of which were misclassified as level walking, 3% as ramp ascend, and 8% as stair ascend. Compared with the prestance phase, it is much more difficult to detect stair descend movement at the preswing.

4.3. Results and Deficiencies of Locomotion Prediction. A simplified HMM model was constructed combining the prior knowledge of steady-state and transient-state observation, and it was defined as follows:

$$\lambda = (S, O, \Pi, A, B), \tag{15}$$

where S denotes the set of hidden states, which refers to the five states of LW, RA, RD, SA, and SD. O is observation sequence, which is obtained from transient-state classifier. $\Pi = [\pi_1, \pi_2, \pi_3, \pi_4, \pi_5]$, where π_i represents the initial probability of the ith (1-LW, 2-RA, 3-RD, 4-SA, 5-SD) state. π_i is set to 0.2 at the beginning of a new cycle, but reset according to steady-state recognition in continuous gaits. $A = [a_{ij}]_{1 \le i,j \le 5}$ is the state transition probability matrix which can be generated from Table 1. $B = [b_{ij}]_{1 \le i,j \le 5}$ is the state observation probability matrix which can be inferred from Table 3. Next, we use Viterbi algorithm to solve the predictive problem of HMM. In this paper, the locomotion prediction only depends on the prior state and transient state, so the algorithm is simplified as the following two steps.

Step 1:

$$\delta_1(i) = \pi_i b_{ij}. \tag{16}$$

Step 2:

$$\begin{aligned} \delta_2(i) &= \max_{1 \le j \le 5} \left[\delta_1 a_{ji}\right] b_{ij}, \\ \psi &= \operatorname{argmax}_{1 \le j \le 5} \left[\delta_1(j) a_{ji}\right], \end{aligned} \tag{17}$$

where i denotes the number of states, j is the observation state, $\delta_{(i)}$ represents the probability of ith locomotion mode, and ψ refers to the upcoming gait with a value of 1, 2, 3, 4, 5, which is the final result for locomotion prediction.

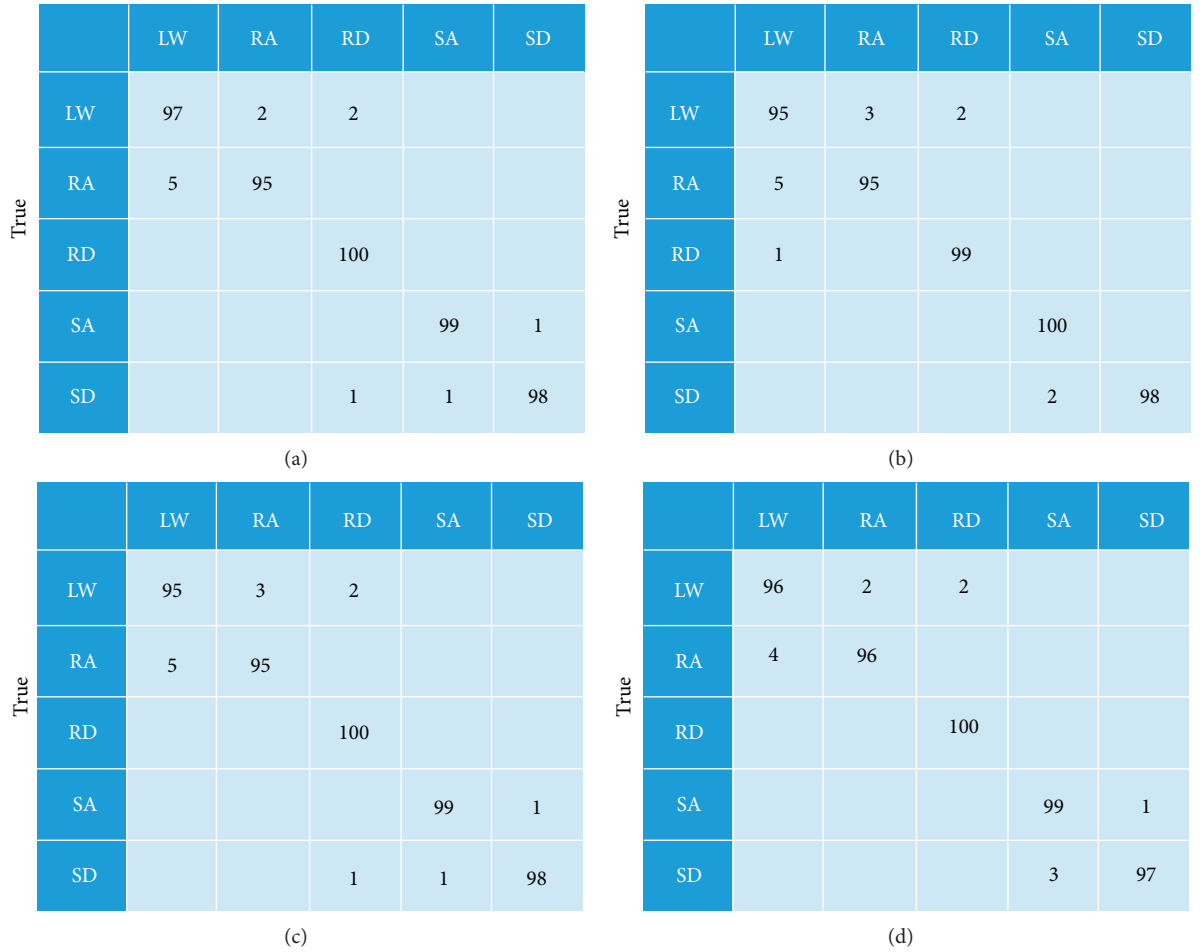

Figure 6: Confusion matrix for steady-state recognition from different classifiers. (a) LDA + SVM confusion matrix estimation. (b) LDA + QDA confusion matrix estimation. (c) LDA + LGBM confusion matrix estimation. (d) LDA + RF confusion matrix estimation.

Table 2: Average accuracy and consumption time of transient-state recognition (unit: %(ms)).

	SVM	QDA	LGBM	RF
Preswing	72.8 (42.3)	49.6 (1.0)	85.1 (14.3)	83.9 (39.7)
Prestance	75.4 (25.6)	49.4 (0.7)	83.5 (11.6)	82.5 (34.1)

By observing the inconsistency between the observed value and the predicted value, we can judge whether the observed value is wrong or not. Combined with the results of steady gait analysis, this method can effectively reduce the misclassification of Table 3. The final predictive accuracy is shown in Table 4, and it improves the accuracy of transient-state recognition from 84.2% to 91.2%.

In addition, because the transition probabilities between level walking to other locomotion modes are all equal to 20%, the prediction accuracy rate for level walking seems not as useful as the other modes. Similarly, the probability of other movements switching to level walking is 50%; if the movement is misclassified as level walking, the error cannot be corrected by using this method. The above two cases are inherent deficiencies of this method.

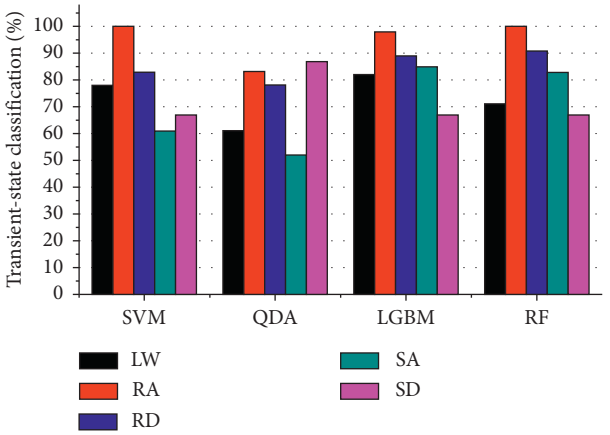

Figure 7: Transient-state recognition at preswing phase.

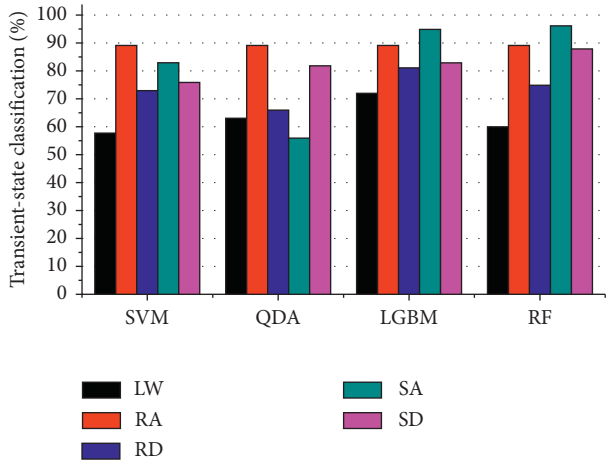

Figure 8: Transient-state recognition at prestance phase.

Table 3: The confusion matrix of LightGBM classifier in preswing transient state.

	LW	RA	RD	SA	SD	Accuracy (%)
LW	82	2	2	4	10	82
RA	0	98	2	0	0	98
RD	4	2	89	4	2	89
SA	0	2	0	85	13	85
SD	23	3	0	8	67	67
Total	—	—	—	—	—	84.2

Table 4: The confusion matrix of LightGBM classifier in transitional state.

	LW	RA	RD	SA	SD	Accuracy (%)
LW	82	2	2	4	10	82
RA	0	100	0	0	0	100
RD	4	0	96	0	0	96
SA	0	0	0	100	0	100
SD	23	0	0	0	78	78
Total	—	—	—	—	—	91.2

5. Conclusions

In this paper, a multilevel classifier fusion strategy based on steady gait recognition and transient-state recognition is proposed to realize human motion intention and prediction under complex environment. The steady-state recognition based on inertial and sEMG fusion as prior gait intention recognition, as well as the LDA + RF classifier, produced over 97.8% accuracy. The transient-state recognition only based on 50 ms sEMG signal as upcoming movement observation and LightGBM classifier outperformed other traditional methods in the accuracy and prediction time, 85.1% accuracy/14.3 ms in the prestance phase and 83.5% accuracy/11.6 ms in the preswing phase. A simplified HMM model that combined prior knowledge and observation was constructed to predict upcoming locomotion with over 91% accuracy. The prediction time could be guaranteed within 70 ms, which ensures that the lower limb prosthesis can switch locomotion in time. The method proposed in this paper can be used in the control of lower limb prosthesis in the future to improve the movement coordination of amputees. In future work, we will consider more application scenarios combined with multisensor information fusion technology.

Data Availability

No data were used to support the study.

Conflicts of Interest

The authors declare that they have no conflicts of interest.

Acknowledgments

This study was supported by the Science and Technology Planning Project of Guangdong Province under grant no. 2016A020220003, Provincial Key Platforms and Major Scientific Research Projects of Guangdong Universities under grant no. 2017KTSCX208, and Science and Technology Planning Project of Zhongshan under grant no. 2019B2066.

References

[1] Z. Li, Y. Yuan, L. Luo et al., "Hybrid brain/muscle signals powered wearable walking exoskeleton enhancing motor ability in climbing stairs activity," *IEEE Transactions on Medical Robotics and Bionics*, vol. 1, no. 4, pp. 218–227, 2019.

[2] H. Su, S. Ertug Ovur, Z. Li et al., "Internet of things (iot)-based collaborative control of a redundant manipulator for teleoperated minimally invasive surgeries," in *Proceedings of the 2020 International Conference on Robotics and Automation (ICRA)*, pp. 9737–9742, IEEE, Paris, France, May–August 2020.

[3] C. Yang, C. Chen, W. He, R. Cui, and Z. Li, "Robot learning system based on adaptive neural control and dynamic movement primitives," *IEEE Transactions on Neural Networks and Learning Systems*, vol. 30, pp. 777–787, 2018.

[4] Y. Liu, W. Su, Z. Li et al., "Motor-imagery-based teleoperation of a dual-arm robot performing manipulation tasks," *IEEE Transactions on Cognitive and Developmental Systems*, vol. 11, pp. 414–424, 2018.

[5] H. Lin, T. Zhang, Z. Chen, H. Song, and C. Yang, "Adaptive fuzzy Gaussian mixture models for shape approximation in robot grasping," *International Journal of Fuzzy Systems*, vol. 21, no. 4, pp. 1026–1037, 2019.

[6] M. Windrich, M. Grimmer, O. Christ, S. Rinderknecht, and P. Beckerle, "Active lower limb prosthetics: a systematic review of design issues and solutions," *BioMedical Engineering OnLine*, vol. 15, p. 140, 2016.

[7] Z. Li, B. Huang, A. Ajoudani, C. Yang, C.-Y. Su, and A. Bicchi, "Asymmetric bimanual control of dual-arm exoskeletons for human-cooperative manipulations," *IEEE Transactions on Robotics*, vol. 34, pp. 264–271, 2017.

[8] H. Huang, T. A. Kuiken, R. D. Lipschutz et al., "A strategy for identifying locomotion modes using surface electromyography," *IEEE Transactions on Biomedical Engineering*, vol. 56, pp. 65–73, 2008.

[9] Z. Li, J. Li, S. Zhao, Y. Yuan, Y. Kang, and C. P. Chen, "Adaptive neural control of a kinematically redundant exoskeleton robot using brain–machine interfaces," *IEEE*

Transactions on Neural Networks and Learning Systems, vol. 30, pp. 3558–3571, 2018.

[10] K. Deok-Hwan, C. Chi-Young, and R. Jaehwan, "Real-time locomotion mode recognition employing correlation feature analysis using emg pattern," *ETRI Journal*, vol. 36, pp. 99–105, 2014.

[11] D. Joshi, B. H. Nakamura, and M. E. Hahn, "High energy spectrogram with integrated prior knowledge for emg-based locomotion classification," *Medical Engineering & Physics*, vol. 37, no. 5, pp. 518–524, 2015.

[12] F. Peng, W. Peng, C. Zhang, and D. Zhong, "Iot assisted kernel linear discriminant analysis based gait phase detection algorithm for walking with cognitive tasks," *IEEE Access*, vol. 7, pp. 68240–68249, 2019.

[13] J. Li, J. Wang, S. Wang et al., "Neural approximation-based model predictive tracking control of non-holonomic wheel-legged robots," *International Journal of Control, Automation and Systems*, pp. 1–10, 2020.

[14] H. Su, Y. Hu, H. R. Karimi, A. Knoll, G. Ferrigno, and E. De Momi, "Improved recurrent neural network-based manipulator control with remote center of motion constraints: experimental results," *Neural Networks*, vol. 131, pp. 291–299, 2020.

[15] J. Li, J. Wang, S. Wang et al., "Parallel structure of six wheel-legged robot trajectory tracking control with heavy payload under uncertain physical interaction," *Assembly Automation*, vol. 40, no. 5, pp. 675–687, 2020.

[16] Z. Liu, W. Lin, Y. Geng, and P. Yang, "Intent pattern recognition of lower-limb motion based on mechanical sensors," *IEEE/CAA Journal of Automatica Sinica*, vol. 4, no. 4, pp. 651–660, 2017.

[17] B.-Y. Su, J. Wang, S.-Q. Liu, M. Sheng, J. Jiang, and K. Xiang, "A cnn-based method for intent recognition using inertial measurement units and intelligent lower limb prosthesis," *IEEE Transactions on Neural Systems and Rehabilitation Engineering*, vol. 27, no. 5, pp. 1032–1042, 2019.

[18] E. C. Wentink, V. G. H. Schut, E. C. Prinsen, J. S. Rietman, and P. H. Veltink, "Detection of the onset of gait initiation using kinematic sensors and emg in transfemoral amputees," *Gait & Posture*, vol. 39, no. 1, pp. 391–396, 2014.

[19] Q. Ai, Y. Zhang, W. Qi, Q. Liu, and a. K. Chen, "Research on lower limb motion recognition based on fusion of semg and accelerometer signals," *Symmetry*, vol. 9, no. 8, p. 147, 2017.

[20] A. J. Young, T. A. Kuiken, and L. J. Hargrove, "Analysis of using EMG and mechanical sensors to enhance intent recognition in powered lower limb prostheses," *Journal of Neural Engineering*, vol. 11, Article ID 056021, 2014.

[21] H. Su, S. E. Ovur, X. Zhou, W. Qi, G. Ferrigno, and E. De Momi, "Depth vision guided hand gesture recognition using electromyographic signals," *Advanced Robotics*, pp. 1–13, 2020.

[22] H. Huang, T. Zhang, C. Yang, and C. P. Chen, "Motor learning and generalization using broad learning adaptive neural control," *IEEE Transactions on Industrial Electronics*, vol. 67, pp. 8608–8617, 2019.

[23] H. Huang, F. Zhang, L. J. Hargrove, Z. Dou, D. R. Rogers, and K. B. Englehart, "Continuous locomotion-mode identification for prosthetic legs based on neuromuscular–mechanical fusion," *IEEE Transactions on Biomedical Engineering*, vol. 58, pp. 2867–2875, 2011.

[24] J. A. Spanias, A. M. Simon, S. B. Finucane, E. J. Perreault, and L. J. Hargrove, "Online adaptive neural control of a robotic lower limb prosthesis," *Journal of Neural Engineering*, vol. 15, Article ID 016015, 2018.

[25] M. Meng, Z. Luo, Q. She, and Y. Ma, "Automatic recognition of gait mode from emg signals of lower limb," in *Proceedings of the 2010 The 2nd International Conference on Industrial Mechatronics and Automation*, vol. 1, pp. 282–285, Beijing, China, May 2010.

[26] C. Yang, C. Chen, N. Wang, Z. Ju, J. Fu, and M. Wang, "Biologically inspired motion modeling and neural control for robot learning from demonstrations," *IEEE Transactions on Cognitive and Developmental Systems*, vol. 11, pp. 281–291, 2018.

[27] J. Li, J. Wang, H. Peng, L. Zhang, Y. Hu, and H. Su, "Neural fuzzy approximation enhanced autonomous tracking control of the wheel-legged robot under uncertain physical interaction," *Neurocomputing*, vol. 410, pp. 342–353, 2020.

[28] X. Wu, Z. Li, Z. Kan, and H. Gao, "Reference trajectory reshaping optimization and control of robotic exoskeletons for human-robot co-manipulation," *IEEE Transactions on Cybernetics*, vol. 50, no. 8, pp. 3740–3751, 2020.

[29] A. Salman, E. G. Allstot, A. Y. Chen, A. M. Dixon, D. Gangopadhyay, and D. J. Allstot, "Compressive sampling of emg bio-signals," in *Proceedings of the 2011 IEEE International Symposium of Circuits and Systems (ISCAS)*, pp. 2095–2098, IEEE, Rio de Janeiro, Brazil, May 2011.

[30] L. Manoni, C. Turchetti, L. Falaschetti, and P. Crippa, "A comparative study of computational methods for compressed sensing reconstruction of emg signal," *Sensors*, vol. 19, no. 16, p. 3531, 2019.

[31] K. Huang, X. Guo, Y. Guo, and G. Wang, "Heterogeneous bayesian compressive sensing for sparse signal recovery," *IET Signal Processing*, vol. 8, no. 9, pp. 1009–1017, 2014.

[32] H. Su, Y. Hu, Z. Li, A. Knoll, G. Ferrigno, and E. De Momi, "Reinforcement learning based manipulation skill transferring for robot-assisted minimally invasive surgery," in *Proceedings of the 2020 IEEE International Conference on Robotics and Automation (ICRA)*, pp. 2203–2208, Paris, France, May–August 2020.

[33] Z. Li, C.-Y. Su, G. Li, and H. Su, "Fuzzy approximation-based adaptive backstepping control of an exoskeleton for human upper limbs," *IEEE Transactions on Fuzzy Systems*, vol. 23, no. 3, pp. 555–566, 2015.

[34] K. Huang, S. Tan, Y. Luo, X. Guo, and G. Wang, "Enhanced radio tomographic imaging with heterogeneous bayesian compressive sensing," *Pervasive and Mobile Computing*, vol. 40, pp. 450–463, 2017.

[35] M. E. Tipping, "Sparse bayesian learning and the relevance vector machine," *Journal of Machine Learning Research*, vol. 1, pp. 211–244, 2001.

[36] S. Ji, Y. Xue, and L. Carin, "Bayesian compressive sensing," *IEEE Transactions on Signal Processing*, vol. 56, no. 6, pp. 2346–2356, 2008.

[37] Z. Li, C. Xu, Q. Wei, C. Shi, and C.-Y. Su, "Human-inspired control of dual-arm exoskeleton robots with force and impedance adaptation," *IEEE Transactions on Systems, Man, and Cybernetics: Systems*, vol. 50, no. 12, pp. 5296–5305, 2018.

[38] H. Su, C. Yang, G. Ferrigno, and E. De Momi, "Improved human-robot collaborative control of redundant robot for teleoperated minimally invasive surgery," *IEEE Robotics and Automation Letters*, vol. 4, no. 2, pp. 1447–1453, 2019.

[39] W. Qi, H. Su, and A. Aliverti, "A smartphone-based adaptive recognition and real-time monitoring system for human activities," *IEEE Transactions on Human-Machine Systems*, vol. 50, no. 5, pp. 414–423, 2020.

[40] H. A. Varol, F. Sup, and M. Goldfarb, "Multiclass real-time intent recognition of a powered lower limb prosthesis," *IEEE*

Transactions on Biomedical Engineering, vol. 57, no. 3, pp. 542–551, 2010.

[41] L. J. Hargrove, G. Li, K. B. Englehart, and B. S. Hudgins, "Principal components analysis preprocessing for improved classification accuracies in pattern-recognition-based myoelectric control," *IEEE Transactions on Biomedical Engineering*, vol. 56, no. 5, pp. 1407–1414, 2009.

[42] H. Su, W. Qi, C. Yang, J. Sandoval, G. Ferrigno, and E. D. Momi, "Deep neural network approach in robot tool dynamics identification for bilateral teleoperation," *IEEE Robotics and Automation Letters*, vol. 5, no. 2, pp. 2943–2949, 2020.

[43] K. H. Ha, H. A. Varol, and M. Goldfarb, "Volitional control of a prosthetic knee using surface electromyography," *IEEE Transactions on Biomedical Engineering*, vol. 58, no. 1, pp. 144–151, 2011.

[44] C. Yang, Y. Jiang, J. Na, Z. Li, L. Cheng, and C.-Y. Su, "Finite-time convergence adaptive fuzzy control for dual-arm robot with unknown kinematics and dynamics," *IEEE Transactions on Fuzzy Systems*, vol. 27, pp. 574–588, 2018.